

The Miscible-Immiscible Quantum Phase Transition in Coupled Two-Component Bose-Einstein Condensates in 1D Optical Lattices

Fei Zhan^{1,2}, Jacopo Sabbatini^{1,2}, Matthew J. Davis¹, and Ian P. McCulloch^{1,2}

¹*School of Mathematics and Physics, The University of Queensland, St. Lucia, QLD 4072, Australia*

²*Centre of Excellence for Engineered Quantum Systems,
The University of Queensland, St. Lucia, QLD 4072, Australia*

(Dated: June 8, 2019)

Using numerical techniques, we study the miscible-immiscible quantum phase transition in a linearly coupled binary Bose-Hubbard model Hamiltonian that can describe low-energy properties of a two-component Bose-Einstein condensate in optical lattices. With the quantum many-body ground state obtained from density matrix renormalization group algorithm, we calculate the characteristic physical quantities of the phase transition controlled by the linear coupling between two components. Furthermore we calculate the Binder cumulant to determine the critical point and draw the phase diagram. The strong-coupling expansion shows that in the Mott insulator regime the model Hamiltonian can be mapped to a spin $1/2$ XXZ model with a transverse magnetic field.

PACS numbers: 64.70.Tg, 03.75.Nt, 03.75.Mn, 67.85.Bc, 05.10.Cc

I. INTRODUCTION

In recent years, progress in single-atom detection and manipulation for ultra-cold neutral atoms has allowed experimentalists to use these systems to engineer and emulate condensed matter systems [1, 2]. Multi-component Bose-Einstein condensates (BEC), formed by atoms of different atomic species or different hyperfine states, has attracted attention from both experimentalists [3, 4] and theorists [5–7] due to their larger symmetry groups and extensive degrees of freedom. As the simplest model consisting of multiple components, the binary BEC has been an appealing candidate to simulate the spin- $1/2$ fermionic superconductor, magnetic behaviour [8], superfluids [9], phase separation [10], quantum phase transitions [11, 12] and thermalization [13].

Binary BECs are naturally divided into miscible and immiscible mixtures based on the interaction strength characterising the system. In a two-component BEC we can observe three kinds of interactions: intra-species interactions for the first component, intra-species interactions for the second component, and inter-species interaction between the two components. If the strength of the inter-species interaction exceeds that of the intra-species interaction, then energy considerations show that the two-components prefer to be in a phase separated or immiscible state [11]. If the opposite is true then the system is said to be in the miscible phase.

A two-component BEC composed of atoms in different hyperfine states can however undergo a miscible-immiscible phase transition controlled by a linear coupling between the energy levels [14]. The experimental flexibility and achievability of this technology have led to the growing volume of research activities in nonlinear Josephson-type oscillations [15], non-topological vortices [16] and non-equilibrium dynamics across the critical point [17].

The dependence of the order parameter on the linear coupling coefficient revealed a second-order transition in

a mean-field (MF) numerical study of this phase transition [14]. The properties of a second order phase transition depend entirely on its universality class and are insensitive to the microscopic details of the underlying system. The universality class is determined by a set of power law indices, called critical exponents which characterize quantities such as the correlation length and the response time of the system [18]. Studies of the static properties of a system near the critical point are challenging because of the divergence of these quantities.

In this paper we study the miscible-immiscible phase transition of a linearly coupled two-component Bose-Hubbard model describing the low energy physics of a binary BEC loaded in an optical lattice.

The exponentially growing size of the Hilbert space as the lattice grows in size prevents the investigation of the full quantum state with exact diagonalization methods even for lattices of moderate sizes. On the other hand, matrix product states (MPS) can parameterize the size of the Hilbert subspace relevant to the low energy properties by the dimension of the matrices, *i.e.* the number of states, and the size of the subspace grows polynomially with the lattice size. In this paper we employ MPS as the ansatz to represent the many-body state and density matrix renormalization group (DMRG) to variationally search the ground-state. Infinite DMRG (iDMRG) methods [19] exploit the system's translational invariance in the thermodynamic limit allowing us to compute the ground state of the system without boundary or finite size effects. From the ground state we can extract a variety of measure like expectation values and multi-point correlations that help us characterize the quantum phase transition and its critical exponents. With the iDMRG methods the correlation length can be calculated directly from the eigenvalues of the transfer matrix.

The paper is organized as following: In Section II, we set up the model Hamiltonian for the numerical calculation and the definitions of order parameter and correlation function. In Section III, we will show the mean occu-

pation number distribution, correlation function, correlation length, phase diagram, and entanglement entropy obtained with a finite system. The calculations with the infinite system and algorithm will be presented in Section IV. In Section V, we illustrate the ground state in a different set of basis states that are categorized by the Z_2 symmetry. We conclude finally in Section VI.

II. MODEL HAMILTONIAN AND SYMMETRIES

The experimental setup we will simulate here is a binary BEC in a 1D optical lattice of lattice constant $L_0 = 1$. The transverse degrees of freedom can be neglected by installing high-frequency transverse modes. The binary BEC consists of two hyperfine atomic states of a single species, which can be defined as spin-up and spin-down, $\sigma = \uparrow, \downarrow$. Spins of two different orientations are coupled by a two-photon transition. This can be realized in an ultra-cold atom gas experiment with e.g. ^{87}Rb atoms [4].

This binary BEC in optical lattice can be mapped to a two-component Bose-Hubbard model Hamiltonian, which is composed of three parts,

$$\hat{H} = \hat{H}_0 + \hat{H}_1 + \hat{H}_C, \quad (1)$$

where the three portions of the total Hamiltonian are given by

$$\hat{H}_0 = -J \sum_{j=1; \sigma}^L \left[a_{j+1, \sigma}^\dagger a_{j, \sigma} + H.c. \right], \quad (2)$$

$$\hat{H}_1 = \frac{U}{2} \sum_{j=1; \sigma}^L n_{j, \sigma} (n_{j, \sigma} - 1) + U_{\uparrow\downarrow} \sum_{j=1}^L n_{j, \uparrow} n_{j, \downarrow}, \quad (3)$$

$$\hat{H}_C = -\Omega \sum_{j=1}^L \left(a_{j, \uparrow}^\dagger a_{j, \downarrow} + a_{j, \downarrow}^\dagger a_{j, \uparrow} \right), \quad (4)$$

respectively. In the above Hamiltonian, $a_{j, \sigma}^\dagger (a_{j, \sigma})$ creates (annihilates) a boson with spin orientation σ on the j th site and $n_{j, \sigma} = a_{j, \sigma}^\dagger a_{j, \sigma}$ is the corresponding occupation number operator. Bosons of either spin species can tunnel to the nearest-neighbour site with the tunnelling element J , assumed here to be the same for both species. Only on-site interactions are included, with coulomb interaction U between same-spin species with $U_{\uparrow\downarrow}$ between different spins. The amplitude of the two-photon microwave coupling between two components is denoted as Ω . In our calculation we define the energy units such that such that $J = 1$.

The interplay of the intra-component interaction or the inter-component interaction determines the phase of the binary BEC [5]. With no inter-species tunneling, $\Omega = 0$, and large intra-component interaction $U > U_{\uparrow\downarrow}$, the total energy is minimized by spreading each components equally to all sites. On the other hand, whenever

$U_{\uparrow\downarrow} > U$ the system phase-separates [20]. A quantity that quantifies this distinction can be defined as [12]:

$$\Delta = \frac{U^2}{U_{\uparrow\downarrow}^2} \quad (5)$$

where $\Delta > 1$ indicates a miscible phase and $\Delta < 1$ is phase-separated.

Turning on the tunneling, $\Omega > 0$, the symmetry is reduced from $U(1) \times U(1)$ to $Z_2 \times U(1)$ and the phase-separated state is replaced by an immiscible phase, analogous to a spin ferromagnet, where the occupation numbers of the species differ but the system remains translationally invariant. For sufficiently large Ω , the system is always in the miscible phase. In this paper, we consider the case $\Delta = 1/4$ and tune Ω to realize the miscible-immiscible phase transition.

In Section III, we consider open boundary conditions (OBC) for a finite system of L sites and N total number of particles. Even though OBC brings forth obstructive boundary effects, it is numerically less expensive than periodic boundary conditions. Indeed, the DMRG algorithm with periodic boundary condition demands additional efforts for an effective simulation [21].

We will focus on the phase transitions with a global filling factor $\rho = N/L = 1$. Such a system in an optical lattice can be appropriately mapped to a single-band Bose-Hubbard model [22, 23].

To look into the miscible-immiscible transition we will study the expectation value and correlation function of the occupation number difference operator, which on the j th site is defined as $\Delta N_j = n_{j, \uparrow} - n_{j, \downarrow}$. Its average expectation value, the magnetization, is,

$$M = \frac{1}{L} \sum_j \Delta N_j. \quad (6)$$

This is the order parameter of the phase transition. Note that neither this order parameter, or the particle number operator for each component, commute with the total Hamiltonian (1).

We also study the correlation function of occupation difference operators between atoms on the j th site and j' th site

$$C(j, j') = \langle \Delta N_j \Delta N_{j'} \rangle. \quad (7)$$

If the system is translationally invariant, $C(j, j')$ only depends on the distance between the two sites $|j - j'|$, and thus we can define $C(j) = C(0, j)$.

It is important to consider the symmetries obeyed by the Hamiltonian. First, the Hamiltonian has the $U(1)$ symmetry as the total number operator N commutes with the Hamiltonian. Note that the number operator for each component does not separately commute with the total Hamiltonian. This can be seen from Hamiltonian H_C that converts bosons from one component to the other and thus the particle number for one component is not conserved. Second, the Hamiltonian has a discrete

\mathbb{Z}_2 symmetry as the Hamiltonian stays unchanged if all the spins are flipped. We will show in the following sections that this symmetry is spontaneously broken when Ω is below the critical value.

III. FINITE SYSTEM

In this paper we will consider the phase transition occurring in Mott insulator regime. Actually the critical point separating the SF and MI regime has not been documented in the literature for a linearly coupled two-component BEC in optical lattices [24]. In the Mott insulator regime the energy scale of the system is dominated by the on-site interaction energy. The coexistence of multiple atoms on a same lattice site is energetically expensive and (only if integer filling factor) thus particles are spread to all the lattice sites equally. Meanwhile the local particle number fluctuation vanishes in ground states. The excited state gapped from the ground state in Mott insulator regime contains pairs of quasi-particle and quasi-hole.

MPS is an excellent ansatz for the ground state of a gapped system. A mean-field derivation can approximate this system in the superfluid regime and predicts the critical value for Ω as [11, 12],

$$\Omega_c = U\rho \left(\frac{1}{\sqrt{\Delta}} - 1 \right). \quad (8)$$

We will show below that MPS with DMRG calculation addresses the MI ground state better than the Mean-field theory and predicts a different power law dependence of Ω_c on U , which agrees with a second-order perturbation theory.

A basic question is still open: where is the border between superfluid regime and Mott insulator regime for this linearly-coupled two-component Bose-Hubbard model? For this two-component model, more degrees of freedom give rise to two branches of quasiparticle spectrum [25]. In the absence of the coupling between the two components, two branches are independent. When a coupling is turned on, one branch accounts for SF-MI transition but the other depends on Ω and is responsible for immiscible-miscible phase transition, which will be addressed in Section V.

The border can be determined by locating the value of on-site interaction where the energy gap closes. The energy gap can be simply verified numerically by calculating the ground state energy E for system of $N-1$, N , and $N+1$ total particles. The system has integer filling factor when the total number of particles is N . The energy gap ΔE can be obtained by the formula,

$$\Delta E = E(N+1) + E(N-1) - 2E(N). \quad (9)$$

Within the numerical accuracy, the numerical simulation gives $\Delta E \neq 0$ for a system with parameters in MI regime. This will be addressed in a subsequent publication [26].

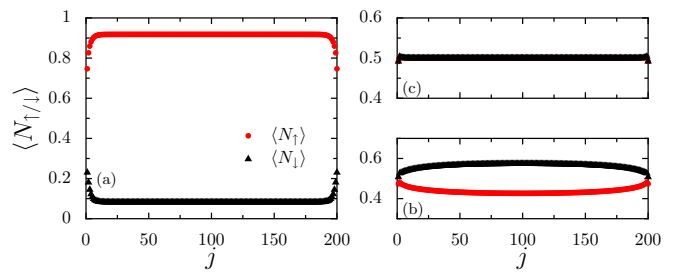


FIG. 1. (Color online) Mean occupation number for spin-up bosons ($\langle N_{\uparrow} \rangle$) (red circles) and spin-down bosons ($\langle N_{\downarrow} \rangle$) (black triangles) on the j th site throughout a 200-site lattice with open boundary condition (a) below, (b) near but still below, and (c) above the critical point in Mott insulator regime. The parameters are (a) $\Omega = 0.18$, (b) $\Omega = 0.214$, and (c) $\Omega = 0.248$.

In the following finite DMRG calculations, we choose the number of states $m = 300$ for the MPS, which is first economical in simulation time and large enough to ensure the variational ground state is close to the true ground state.

A. Occupation distribution

We first show the immiscible and miscible phases by displaying the occupation distribution throughout a lattice. In Fig. 1, we plot the mean occupation number for both components below, near but still below, and above the critical point.

When $\Omega \ll \Omega_c$, the system is in the immiscible phase. In immiscible phase, the largest energy scale in the system is the inter-component interaction strength. The coexistence of different component bosons costs more energy, therefore states with only one component on each sites are favourable. The states which have spin-up bosons on one site is degenerate with a state with spin-down bosons. As a result, the system has to choose one of the two states randomly.

The randomness can be manifested in Fig. 1. In a real-life numerical simulation many factors, e. g., the direction of DMRG variational algorithm, may determine which component will appear in the favourable states. In order to show the randomness, for each values of Ω we start the DMRG simulation with a different random initial wave function. The probability that one of the two components is preferred by random fluctuation is one half. Consequently, when the system is in immiscible phase we saw the domination of spin-up bosons in half of the simulations and the domination of spin-down bosons in the other half. We give here two representatives in Fig. 1. In Fig. 1(a), spin-up bosons dominate the occupation across the entire lattice, while in Fig. 1 (b) the opposite species dominates.

We recall the total Hamiltonian (1) preserves the \mathbb{Z}_2 symmetry, for it stays unchanged when all spin orien-

tations are flipped. Obviously the “ground” state in immiscible phase does not preserve the \mathbb{Z}_2 symmetry of the total Hamiltonian with the imbalance $\langle \Delta N \rangle$ in mean occupation numbers for two components. This is \mathbb{Z}_2 spontaneous symmetry breaking. In the thermodynamic limit, the ground state is 2-fold degenerate. In the ground state subspace, the DMRG variational calculation adopts the lowest-entropy state and therefore numerically enforces the order of the symmetry breaking state. In principle for a finite size system spontaneous symmetry breaking should not occur. However in a numerical DMRG calculation the broken symmetry state is variationally favoured if the energy splitting of the groundstate is smaller than an energy scale set by the truncation error of the calculation.

When the control parameter Ω becomes larger, the imbalance in occupation decreases to zero at critical point, as can be seen in Fig. 1(b). Above the critical point, the ground state has the same \mathbb{Z}_2 symmetry of the Hamiltonian and both components occupy equally on all of the sites. Therefore the imbalance must be zero and the system is in the miscible phase, see Fig. 1(c).

One must always be aware of the boundary effects when we approximate a system in thermodynamic limit with a finite system. The boundary effect comes from the correlation between a particle in the bulk of the finite system and a particle on the boundary, where particles can only hop in one direction. As we can see in Fig. 1(a), near the boundary the mean occupation number for both spin-up and spin-down bosons deviate from the magnitude for the bulk sites. It lowers partially the mean occupation number of the dominating component and raises that for the other component. Approaching the critical point, the correlation between two sites at longer distance starts to be non-negligible, as we expect for a second-order phase transition. Consequently the boundary effect influences more strongly the sites deep into the bulk of the lattice, which can be seen in Fig. 1(b). When the control parameter is sufficiently close to the critical point, the influence of both boundaries merge together, we see two curved lines for the mean occupation number of both components. The boundary effect is negligible when it is above the critical point, see Fig. 1(c). The effect of the boundaries on the calculation of correlation function is explored in more detail in the following subsection.

In Fig. 2, we show the absolute imbalance $\langle \Delta N_{L/2} \rangle$ as the function of the coupling coefficient Ω for some different lattice sizes. As we have discussed above, below the critical value Ω_c the imbalance is nonzero and drops off quickly down to zero around the critical point. We can also see Ω_c shows clear saturating behavior as the lattice size is increased. The increasing rate slows down and Ω_c saturates asymptotically in the thermodynamic limit. From Fig. 2, the critical point can be estimated as $\Omega_c \approx 0.215$. We improve on this estimate in section III C below.

By using finite sizing scaling, one can extract the crit-

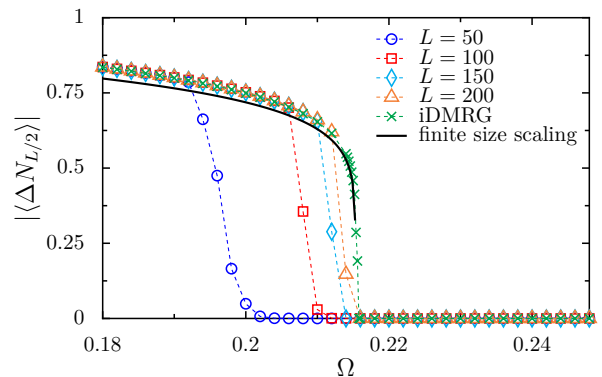


FIG. 2. (Color online) The occupation imbalance $\langle \Delta N \rangle$ on the middle site $L/2$ of lattices having 50 (blue circle), 100 (red square), 150 (cyan diamond), and 200 (orange triangle) sites as the function of the coupling coefficient Ω . The green crosses are the data for an infinite lattice from infinite DMRG calculation. The dashed lines are used to guide eyes. The solid black line is drawn with parameters from a finite size scaling about the critical point with exponent $\beta = 1/8$.

ical coupling Ω_c and critical exponents by collapsing curves for lattices of different lengths. First we define the reduced coupling $\epsilon = |1 - \Omega/\Omega_c|$. Previous studies in the literature has indicated this phase transition is of second order [14]. Near the critical point of a second-order phase transition, we know that the correlation length and magnetization satisfy $\xi \propto \epsilon^{-\nu}$ and $M \propto \epsilon^\beta$ (only below the critical point, otherwise $M = 0$), from which we can deduce the relation $M \propto \xi^{-\beta/\nu}$. For a finite lattice, instead of approaching zero when ξ diverges M stays at a finite nonzero value when ξ becomes comparable to the lattice length L . This behavior can be described by $M = \xi^{-\beta/\nu} M_0(L/\xi)$ with the assisting function $M_0(x)$ that goes to zero as $x^{-\beta/\nu}$ when $x \rightarrow \infty$ and a constant when $x \rightarrow 0$. To remove the size dependence, we define the scaling function

$$\tilde{M}(L^{1/\nu} \epsilon) = L^{\beta/\gamma} M(\epsilon). \quad (10)$$

With $\nu = 1$ and $\Omega_c = 0.2153$ we will obtain in the next subsections, we find four curves for the four lengths coalesce with $\beta = 1/8$. In Fig. 2, we plot the curve ϵ^β with $\beta = 1/8$ obtained from the finite size scaling and $\Omega_c = 0.2153$. We find near the transition point it agrees very well with the results from iDMRG calculations in Section IV.

B. Correlation function and correlation length

Close to the boundary the quantum state may locally deviate dramatically from the quantum state in the thermodynamic limit, due to the inevitable boundary effect, see the mean occupation in Fig. 1. For these reasons, in order to simulate the correlation in the thermodynamic limit with a finite size system, we only investigate the

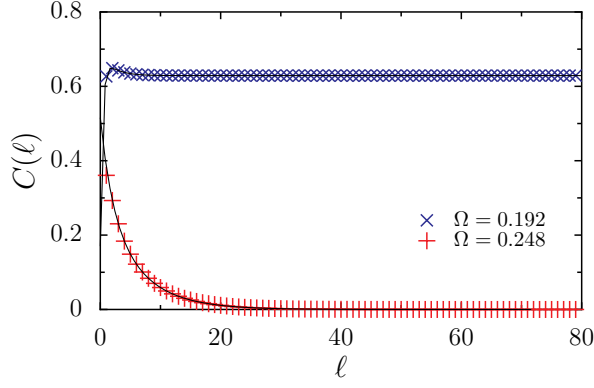


FIG. 3. (Colour online) The correlation function $C(\ell)$ calculated in the bulk of a lattice with 200 sites with 60 sites cut off at both ends. The blue crosses (red pluses) are the values of the correlation function between the zeroth site and the ℓ th site when $\Omega = 0.192$ ($\Omega = 0.248$), which is below (above) the critical point. The curves are the fittings with respect to a sum of multiple exponential functions.

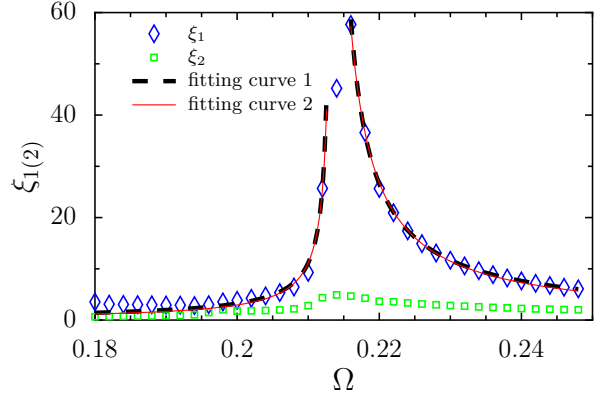


FIG. 4. (Colour online) The first (blue diamond) and second (green square) longest correlation lengths extracted by fitting the correlation function with the sum of multiple exponential functions for a lattice of 200 sites. The longest correlation length shows divergence in a region for the control parameter Ω . The black dashed line shows the fitting curve with the critical exponent ν as an independent variable and the red solid line shows the fitting curve with the plausible fixed exponent $\nu = 1$, see text.

correlation function computed in the bulk of the lattice, where boundary effect can be neglected. Keeping this in mind is particularly important when $\Omega < \Omega_c$, see Fig. 1(a). Very close to critical point, the region where boundary effects can be neglected is very small or does not exist. For this case, the correlation function is not reliable for extracting the correlation length. For instance, to calculate the two-point correlator (7) in Fig. 3 for a lattice of 200 sites, we cut off 60 sites at both ends of the lattice. Therefore the correlation function ranges up to 80 sites in Fig. 3, and the correlation function only depends on the distance $|j - j'|$ between its two ends. Consequently we only enumerate the distance by $\ell = |j - j'|$. When

$\Omega = 0.192 \ll \Omega_c$, in Fig. 3, we find within a few sites the correlation function first increases and then decreases exponentially and saturates at a nonzero value. This shape of the correlation correlation stems from a finite size effect which does not occur in infinite DMRG calculations. While $\Omega = 0.248 \gg \Omega_c$, in the miscible phase, the correlation function exponentially decays to zero.

As suggested by the characteristic form of correlation functions in MPS [27] and the fact that correlation decays exponentially in a system off criticality, we fit the correlation function with a sum of exponential functions:

$$C(\ell) = \sum_i a_i \exp(-\ell/\xi_i) + c, \quad (11)$$

where the constant c has a nonzero value when Ω is below the critical point. We find in Fig. 3 that the fitting precisely captures the behaviours of the correlation function.

In Fig. 4, we plot the first two longest correlation lengths ξ_1 and ξ_2 from the fitting function (11). We can see even the second longest correlation length stays finite across the whole space of Ω . The longest correlation length shows clear divergent behaviour around $\Omega = 0.215$, which characterizes the behaviour of the system close to criticality. In addition, we fit the correlation length with the power law $\xi \propto |\Omega - \Omega_c|^{-\nu}$ around critical point. In the first fitting, shown in Fig. 4, we set ν as an independent variable and obtain the following optimized fitting function:

$$\xi_1(\Omega) = \begin{cases} \frac{0.07}{|0.2133 - \Omega|^{0.88}} & : \Omega < \Omega_c \\ \frac{0.28}{|0.2131 - \Omega|^{0.915}} & : \Omega > \Omega_c. \end{cases}$$

On account of the nonlinear least square algorithm's numerical complexity, combined with the less reliable data adjacent to the transition point, the exponent ν may have low numerical accuracy. Nevertheless, they are very close to the already known value $\nu = 1$ for the conformal field theory for the 1D quantum Ising model with a transverse magnetic field. Therefore for a second fitting, also shown in Fig. 4, we set $\nu = 1$ as a constant and obtain:

$$\xi_1(\Omega) = \begin{cases} \frac{0.03}{|0.2135 - \Omega|} & : \Omega < \Omega_c \\ \frac{0.2}{|0.2125 - \Omega|} & : \Omega > \Omega_c. \end{cases}$$

The similarity of these two fit functions in Fig. 4 shows the difficulty in obtaining accurate values of ν and Ω_c by this method. The critical point $\Omega_c = 0.213$ is somewhat below the result obtained from Fig. 2, and shows the accuracy scale of this fitting technique. The fitting for the parameter above the critical point is better than the other side in the control parameter space. The reason should be the more severe boundary effect below the critical point. It can be seen in Fig. 4 that both fittings overlap with the data point very well, only slightly deviating when the control parameter is far away from the critical point. In any event, this suggests that $\nu = 1$ should be probable, as consistent with already known theories.

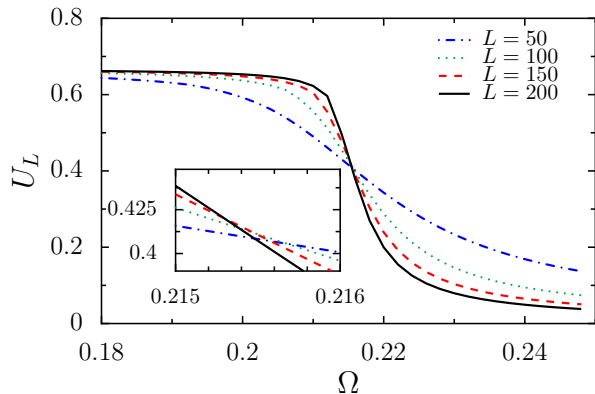


FIG. 5. (Color online) The Binder cumulant as a function of the control parameter Ω for lattices of $L = 50$ (blue dash-dotted), 100 (green dotted), 150 (red dashed), and 200 (black solid). The inset zooms into the region where four curves cross each other.

C. Binder cumulant

To determine the critical point more accurately from finite-size calculations, the Binder cumulant is a better tool than the naive finite size scaling, which was proposed and has found applications in the quantum Monte Carlo community [28, 29]. Its potential usefulness and generalizations still attract a lot of attention [30, 31]. With the Binder cumulant the critical point can be determined with a relatively small finite size lattice. For example, the critical temperature for a two-dimensional Ising model can be obtained by Binder cumulant with a 9×9 lattice [28].

The Binder cumulant U_L is defined as

$$U_L = 1 - \frac{\langle M^4 \rangle}{3\langle M^2 \rangle^2}, \quad (12)$$

where $\langle M^2 \rangle$ and $\langle M^4 \rangle$ are the second-order and the fourth-order moments of the order parameter, respectively. Note that Binder cumulant depends on the length of the lattice L .

In Fig. 5, we plot the Binder cumulant with the same parameters we have used for the above calculations for lattices of a variety of lengths. The curves clearly show the asymptotic behaviour of Binder cumulant: It decreases in the space of control parameter and approaches asymptotically to $2/3$ and 0 below and above the critical point, respectively; Around the critical point, it decreases faster than in other region; In addition, the data for longer lattice decreases faster than that for shorter lattice. As a result, the different curves will cross each other around the critical point. In the thermodynamic limit the curve should be discontinuous at the critical point.

As we can see in Fig. 5, the four curves cross each other at one point. The inset of Fig. 5 shows the crossing points locate in a region $[0.2152 \ 0.2158]$. The value of Ω

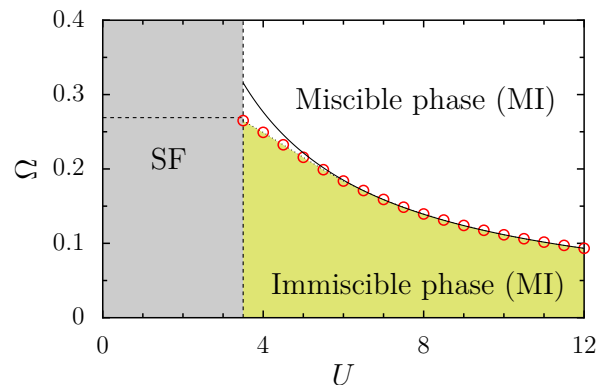


FIG. 6. (Color online) The phase diagram in the space of control parameter Ω and onsite intracomponent interaction U . The interspecies interaction $U_{\uparrow\downarrow} = 2U$. The border between superfluid and Mott insulator will be updated in upcoming works. The red circles are the data points of the border between miscible and immiscible phases determined by Binder cumulant for lattices of $L = 50$ and $L = 100$. The dotted curve connecting the red circles is interpolated from the data points (red circle). The solid curve is attained by fitting the data points with $1/U$ where U is larger than 10.

for the crossing point corresponds the critical value Ω_c . The cubic spline interpolation of the curves for $L = 150$ and 200 suggests the critical point should be at $\Omega_c = 0.2153$. In the Subsection III A, we performed the finite size scaling with this value as the tentative critical value and obtained the expected value for the exponent β . We will see this value also agrees with the iDMRG results in the following section.

D. Phase diagram

As we have seen in the last subsection Binder cumulant can locate the critical point very precisely, and using this measure we now plot the phase diagram of this model Hamiltonian.

In Fig. 6, we depict the phase diagram in the space of Ω_c and U , while keeping $U_{\uparrow\downarrow} = 2U$, corresponding to $\Delta = 1/4$. In Fig. 5, we can find that increasing the number of lattice sites only changes the value of Ω_c in the fourth digit after the decimal point. In consequence, to speed the calculation, we locate Ω_c by using Binder cumulants for shorter lattices between $L = 50$ and $L = 100$.

We can find in Fig. 6 for the MI regime the critical value Ω_c decreases as U increased as approximately $1/U$. This result is in contrast to mean-field predictions, which shows linear dependence of Ω_c on U [12].

When U and $U_{\uparrow\downarrow}$ are large, the tunneling between sites is negligible and therefore can be considered as a perturbation. Perturbation theory can be employed to find a further approximation aiming for more insights of the underlying physics. Using the strong-coupling expan-

sion, we derived the effective Hamiltonian for this model, which turns out to be a ferromagnetic XXZ model with a transverse magnetic field:

$$H = -J_{\perp} \sum_j [S_j^x S_{j+1}^x + S_j^y S_{j+1}^y] + J_z \sum_j S_j^z S_{j+1}^z + \Gamma \sum_j S_j^x, \quad (13)$$

where S_j^x , S_j^y , and S_j^z are the three components of the spin-operator for a spin 1/2 particle on the j th lattice site, respectively.

The coefficients for the effective Hamiltonian are

$$J_{\perp} = \frac{4}{U_{\uparrow\downarrow}}, \quad J_z = \frac{4}{U_{\uparrow\downarrow}} - \frac{8}{U}, \quad \Gamma = -2\Omega. \quad (14)$$

For the parameters we have chosen $U_{\uparrow\downarrow} = 2U$, *viz.* $|J_z/J_{\perp}| = 3$, which indicates the ferromagnetic ground state when $\Omega = 0$. When $|J_z/J_{\perp}| \rightarrow \infty$, *i.e.*, the first term in Eq. (13) can be neglected, this model can be further mapped into the Ising model in a transverse magnetic field, for which we know the phase transition occurs at $\Gamma_c = J_z/2$. For non-zero J_{\perp} , the exact dependence of Γ_c on J_{\perp} and J_z is not known, but we expect that $\Gamma_c \propto 1/U$.

In Fig. 6, in the region where $U > 10$ we fit the data points on the border line between miscible and immiscible phase to the function C/U and find the coefficient $C \approx 1.09$, in excellent agreement with what we obtained from the DMRG calculation for XXZ with transverse field, where we found $\Gamma_c = 0.36J_z$. Since $J_z = -6/U$, we obtain $\Gamma_c = 2.16/U$ and $\Omega_c = 1.08/U$.

E. Entanglement entropy

It has been demonstrated that the concept of entanglement entropy, which is a significant concept in quantum information, also plays an important role in understanding quantum phase transition in the condensed matter physics. It is responsible for the appearance of long-range correlation [32, 33]. The bipartite entanglement entropy can capture the large-scale behaviour of quantum correlations at a critical regime. In the vicinity of the critical point Ω_c , the entanglement entropy diverges logarithmically with the correlation length. Here we will present the scaling behaviour of entanglement entropy for the model and determine the central charge at criticality.

Suppose the lattice is divided bipartitely into the sublattice A and the sublattice B . The entanglement entropy is then defined as the Von Neumann entropy of either one of the two sublattices, say the sublattice A ,

$$S = -\text{Tr}(\rho_A \log(\rho_A)), \quad (15)$$

where $\rho_A = \text{Tr}_B(\rho)$ is the reduced density matrix for the part A .

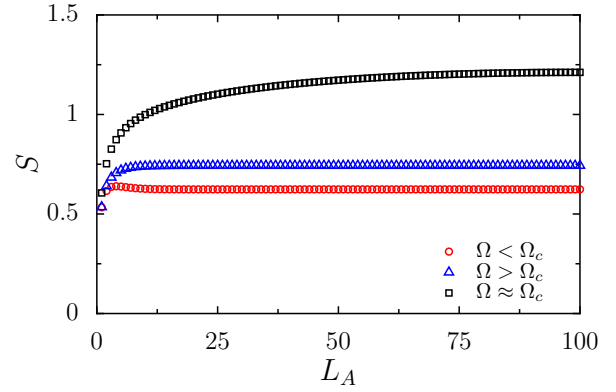


FIG. 7. (Color online) The entanglement entropy up to the half of a 200 sites lattice, below, near, and above the critical point in Mott insulator regime. The curve with $\Omega \approx \Omega_c$ is fitted with Eq. (16).

In Fig. 7, we plot the entanglement entropy for $\Omega < \Omega_c$, $\Omega \approx \Omega_c$, and $\Omega > \Omega_c$ as the size of the sublattice A is increased up to the half of the whole lattice. We can find the bipartite entanglement entropy increases as the block size increases. When it is off-critical, entanglement entropy saturates above some critical length which is proportional to the correlation length ξ in the Subsection III B.

In Ref. [33], the critical entanglement entropy is shown to coincide with the entropy in CFT for a range of spin chains. Consequently, central charge can be extracted from the critical entanglement entropy. As derived in [34], the critical entanglement entropy satisfies

$$S \approx \frac{c + \bar{c}}{6} \log \left[\frac{2L}{\pi} \sin \left(\frac{\pi L_A}{L} \right) \right] + k, \quad (16)$$

for a finite lattice of total size L and a sublattice of size L_A with periodic boundary conditions, where c and \bar{c} are holomorphic and antiholomorphic central charges of the conformal field theory and k is a model-dependent constant. For open boundary conditions, only the holomorphic central charge is expected.

We should point out the model-dependent constant k here is generally nonzero, unlike the other widely studied models. For instance, in the quantum Ising model, the ordered state with zero or infinite transverse field is a product state. The entanglement entropy of such a totally ordered state is zero and therefore $k = 0$. Nevertheless, for the two-component Bose-Hubbard model the entanglement entropy away from the critical point approaches that of the gapped MI system when $\Omega \rightarrow 0$. This is vanishing only when $(U, U_{\uparrow\downarrow}) \rightarrow \infty$; otherwise the remaining local particle number fluctuation contributes to the entanglement entropy as a correction to the CFT prediction.

In extracting the central charge, we find difficulties caused by the open boundary conditions. For this reason, we use periodic boundary conditions. For the XXZ

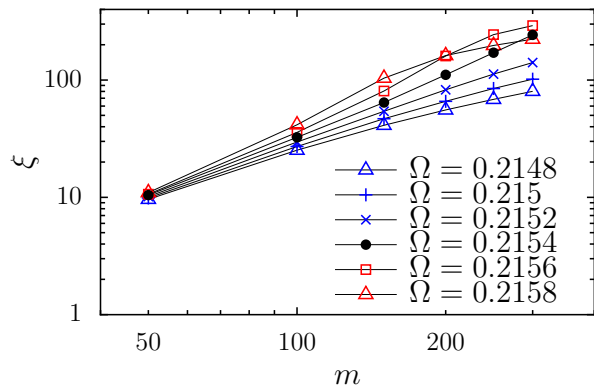


FIG. 8. (Color online) Correlation length vs. number of states for various values of the coupling coefficient Ω around the critical point in Mott insulator regime. The other parameters are $U = 5, U_{\uparrow\downarrow} = 10$.

Hamiltonian (13), from our numerical calculation we confirmed the central charge $c = 1/2$, corresponding to the universality class of the transverse-field Ising model. For the Hamiltonian (1) with periodic boundary condition, we also successfully extracted the central charge $c = 1/2$ when $U \rightarrow \infty$, consistent with the critical exponents we obtained above.

IV. SIMULATIONS WITH iDMRG

So far we have simulated a system only for a finite size lattice. The expectation value of the physical quantities are therefore affected by finite size effects and the boundary effects that breaks the translational invariance of a system. To remove these drawbacks, we now use the infinite DMRG that is a better ansatz for a translational invariant system.

In Fig. 2, the green crosses show the mean occupation number imbalance obtained from iDMRG [19] calculations. We can see it matches very closely the asymptotic result of the finite DMRG calculation for the critical point.

Since the translational invariance of the lattice, the representing matrices in MPS are all equivalent. Besides the fact that the correlation length can be extracted from the correlation function, it can also be directly calculated from the spectrum of the transfer matrix, which originates from the exponential decay nature of MPS [27, 35].

The correlation length obtained this way increases as the number of states m (dimension of MPS representation) increased. For a gapped noncritical system, it saturates at a certain value of m , while for a gapless critical system it diverges with m . Fig. 8 shows this dependence in a logarithmic plot. Up to $m = 300$, all the curves have shown the expected saturation behaviour except the curve for $\Omega = 0.2154$. Therefore, the critical point is the closest to $\Omega = 0.2154$, which is very close to the value $\Omega_c = 0.2153$ from the Binder cumulant for finite systems.

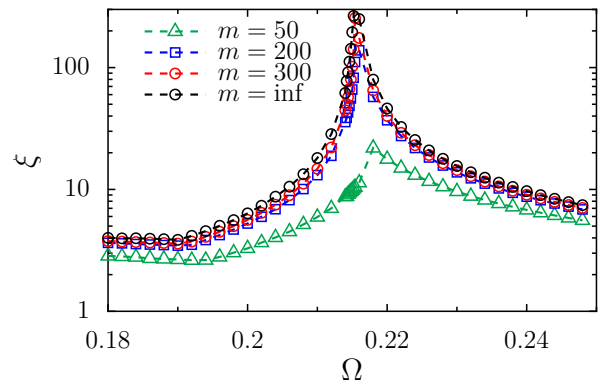


FIG. 9. (Color online) The correlation length obtained from iDMRG calculation for a translationally invariant infinite lattice with the increasing size of number of states: $m = 50$ (green triangle), $m = 200$ (blue square), $m = 300$ (red circle), and $m = \text{Inf}$ (black circle). The data for $m = \text{Inf}$ is obtained by extrapolation.

In Fig. 9, we plot the correlation length as a function of Ω as number of states $m = 50, 200$, and 300 . When $m = 50$, correlation length are longer around the critical point but the divergent behaviour has not been obvious. It becomes obvious since $m = 200$. We also plot the correlation length when m is extrapolated to infinity in Fig. 9. A fitting of it with function $\xi \propto |\Omega - \Omega_c|^{-\nu}$ gives ν equals 0.94, which is close to the known value $\nu = 1$ for the conformal field theory for 1D quantum Ising model with a transverse magnetic field, and a much better approximation than the fitted correlation length for finite size calculations presented in section III B above.

V. $U(1)$ - \mathbb{Z}_2 SYMMETRY

The total Hamiltonian (1) satisfies \mathbb{Z}_2 symmetry because it remains unchanged if all spins are flipped. The ground state should preserve the same \mathbb{Z}_2 symmetry to be symmetric or anti-symmetric, although this is not the case for symmetry breaking state when $\Omega < \Omega_c$. However, we can always unitarily transform the Hilbert space composed of product Fock states into one composed of symmetric and antisymmetric basis states. The new Hilbert space can provide us new insights into how the \mathbb{Z}_2 symmetry is broken and restored across the critical point.

This unitary transformation brings the operators to the ones specified on symmetric and anti-symmetric states in the following way,

$$b_s = \frac{1}{\sqrt{2}}(a_{\uparrow} + a_{\downarrow}) \quad (17)$$

$$b_a = \frac{1}{\sqrt{2}}(a_{\uparrow} - a_{\downarrow}). \quad (18)$$

The reversed relation can be obtained by simple linear

combinations,

$$a_{\uparrow} = \frac{1}{\sqrt{2}}(b_s + b_a) \quad (19)$$

$$a_{\downarrow} = \frac{1}{\sqrt{2}}(b_s - b_a). \quad (20)$$

The choice of coefficient $1/\sqrt{2}$ preserves the commutator relation,

$$[b_{s(a)}, b_{s(a)}^{\dagger}] = 1. \quad (21)$$

Substituting (19) and (20) into the three portions of the total Hamiltonian (1), we have the Hamiltonian in terms of $(b_{s(a)}^{\dagger}, b_{s(a)})$ operators.

First the non-interacting part,

$$\hat{H}_0 = -J \sum_{j=1}^L \sum_{p=s,a} [b_{j+1,p}^{\dagger} b_{j,p} + H.c.]. \quad (22)$$

As no spin-flipping exists in the original Hamiltonian (2), symmetry is expected to be conserved during the tunnelling.

The on-site interaction Hamiltonian between the particles of the same component transforms to,

$$\begin{aligned} \hat{H}_U = & \frac{U}{4} \sum_j \sum_{p=s,a} N_{j,p}(N_{j,p} - 1) \\ & + \frac{U}{4} \sum_j (b_{j,s}^{\dagger} b_{j,s}^{\dagger} b_{j,a} b_{j,a} + b_{j,a}^{\dagger} b_{j,a}^{\dagger} b_{j,s} b_{j,s}) \\ & + U \sum_j N_{j,s} N_{j,a}, \end{aligned} \quad (23)$$

where $N_{j,p} = b_{j,p}^{\dagger} b_{j,p}$ is the number operator for the symmetric state ($p = s$) or the antisymmetric state ($p = a$). The Hamiltonian between the two components becomes,

$$\begin{aligned} \hat{H}_{U\uparrow\downarrow} = & \frac{U_{\uparrow\downarrow}}{4} \sum_{j=1}^L [N_{j,s}(N_{j,s} - 1) + N_{j,a}(N_{j,a} - 1) \\ & - (b_{j,s}^{\dagger} b_{j,s}^{\dagger} b_{j,a} b_{j,a} + b_{j,a}^{\dagger} b_{j,a}^{\dagger} b_{j,s} b_{j,s})]. \end{aligned} \quad (24)$$

These two interaction Hamiltonian contain terms that annihilate pairs of symmetric bosons and create pairs of anti-symmetric bosons, and vice versa, but with opposite sign. Therefore, \hat{H}_U and $\hat{H}_{U\uparrow\downarrow}$ are two competing terms. The intra-component interaction \hat{H}_U favours symmetric states for the less co-existence of same spin bosons at a same site. On the contrary, the inter-component interaction $\hat{H}_{U\uparrow\downarrow}$ will be lower for the asymmetric state.

The linear coupling Hamiltonian between two components becomes,

$$\hat{H}_C = -\Omega \sum_j (N_{j,s} - N_{j,a}). \quad (25)$$

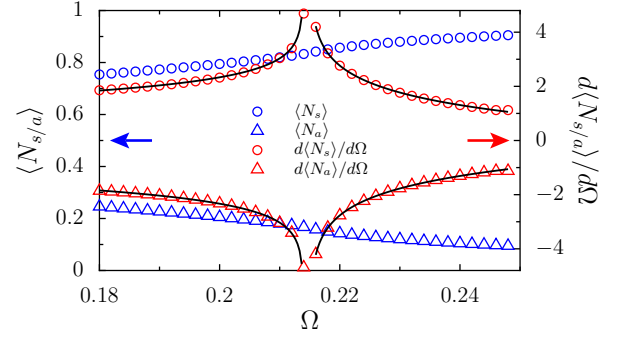


FIG. 10. (Colour online) The mean occupation numbers and its derivatives with respect to Ω for symmetric states and anti-symmetric states around the critical point. The black solid curves are the fitting curves for the derivatives to a logarithmic function. The arrows point to the corresponding y -axis of mean occupation number or its derivative.

This term effectively has the function of an unbalanced chemical potential, favouring particles in the symmetric state as Ω is increased.

We also employ the iDMRG algorithm to obtain the optimized iMPS with the Hamiltonian given above. In Fig. 10, we plot the mean occupation number for symmetric and anti-symmetric states. As expected from the analysis of the linear coupling Hamiltonian, more and more bosons occupy the symmetric states with increasing Ω . There is a kink around the critical point Ω_c . To see this kink more closely, we also plot the derivative of the curve. At the critical point, the derivative diverges.

We find the derivative of the mean occupation number both for symmetric and anti-symmetric states can be fitted with a logarithmic function, as shown by the solid curves in Fig. 10. This is another numerical evidence that the linearly coupled two-component Bose-Hubbard model we are studying is equivalent to a 1D quantum Ising model with transverse magnetic field, which gives the critical exponent $\alpha = 0$ [18].

VI. CONCLUSION

In this paper we comprehensively study the miscible-immiscible phase transition in a linearly coupled two-component Bose-Hubbard model. We focus on this model in Mott insulator regime with integer filling factor one, *i.e.*, the total number of particles equal to number of lattice sites. We simulate this system by using both finite DMRG or iDMRG algorithms.

We have demonstrated basic features of this phase transition. Below the transition point the symmetry breaking states show imbalanced mean occupation number. The imbalance decreases and disappears at the transition point. Above the transition point the imbalance remains zero and the \mathbb{Z}_2 symmetry of flipping the spins is restored in the ground state. The correlation functions of the occupation imbalance operator show exponential

decay when it is off-critical. The extracted correlation length diverges with power-law exponent ν close to one, and critical exponents $\beta = 1/8$ and $\alpha = 0$.

We employed the Binder cumulant to determine the critical value of linear tunneling coefficient, and determined the phase diagram. A strong-coupling expansion unveils that in Mott insulator regime this model is equivalent to a XXZ model with a transverse magnetic field.

The phase transition is also characterized by the entanglement entropy, which diverges logarithmically at the critical point and otherwise saturates. The central charge at the critical point was extracted from DMRG calculations with periodic boundary conditions. All of these

results demonstrate conclusively that the transition is in the universality class of the $c = 1/2$ conformal field theory.

ACKNOWLEDGMENTS

This work has been supported by the Australian Research Council Centre of Excellence for Engineered Quantum Systems and the Discovery Projects funding scheme (Project No. DP1092513). After completion of this manuscript, we became aware of a new work [36] looking at this model in the superfluid regime.

-
- [1] M. Greiner, O. Mandel, T. Esslinger, T. W. Hänsch, and I. Bloch, *Nature* **415**, 39 (2002).
 - [2] I. Bloch, J. Dalibard, and S. Nascimbène, *Nat. Phys.* **8**, 267 (2012).
 - [3] J. Stenger, S. Inouye, D. M. Stamper-Kurn, H.-J. Miesner, A. P. Chikkatur, and W. Ketterle, *Nature* **396**, 345 (1998).
 - [4] D. S. Hall, M. R. Matthews, J. R. Ensher, C. E. Wieman, and E. A. Cornell, *Phys. Rev. Lett.* **81**, 1539 (1998).
 - [5] T.-L. Ho and V. B. Shenoy, *Phys. Rev. Lett.* **77**, 3276 (1996).
 - [6] H. Pu and N. P. Bigelow, *Phys. Rev. Lett.* **80**, 1130 (1998).
 - [7] E. Timmermans, *Phys. Rev. Lett.* **81**, 5718 (1998).
 - [8] B. Paredes and J. I. Cirac, *Phys. Rev. Lett.* **90**, 150402 (2003).
 - [9] A. Kuklov, N. Prokof'ev, and B. Svistunov, *Phys. Rev. Lett.* **92** 030403 (2004).
 - [10] O. E. Alon, A. I. Streltsov, and L. S. Cederbaum, *Phys. Rev. Lett.* **97**, 230403 (2006).
 - [11] J. Sabbatini, W. H. Zurek, and M. J. Davis, *Phys. Rev. Lett.* **107** 230402 (2011).
 - [12] J. Sabbatini, W. H. Zurek, and M. J. Davis, *New J. Phys.* **14**, 095030 (2012).
 - [13] J. M. Zhang, C. Shen, and W. M. Liu, *Phys. Rev. A* **85**, 013637 (2012).
 - [14] I. M. Merhasin, B. A. Malomed, and R. Driben, *J. Phys. B: At. Mol. Opt. Phys.* **38**, 877 (2005).
 - [15] J. Williams, R. Walser, J. Cooper, E. Cornell, and M. Holland, *Phys. Rev. A* **59**, R31 (1999).
 - [16] Q.-H. Park and J. H. Eberly, *Phys. Rev. A* **70**, 021602 (2004).
 - [17] C. Lee, *Phys. Rev. Lett.* **102**, 070401 (2009).
 - [18] J. Cardy *Scaling and Renormalization in Statistical Physics* (Cambridge University Press), (1996).
 - [19] I. P. McCulloch arxiv:0804.2509 (2008).
 - [20] F. Zhan and I. P. McCulloch arXiv:submit/0936630 (2014).
 - [21] P. Pippin, S. R. White, and H. G. Evertz, *Phys. Rev. B* **81**, 081103 (2010).
 - [22] D. van Oosten, P. van der Straten, and H. T. C. Stoof, *Phys. Rev. A* **67**, 033606 (2003).
 - [23] M. Greiner, I. Bloch, O. Mandel, T. W. Hänsch, and T. Esslinger, *Phys. Rev. Lett.* **87**, 160405 (2001).
 - [24] But see Ref. [36] for some recent work.
 - [25] P. Tommasini, E. J. V. de Passos, A. F. R. de Toledo Piza, M. S. Hussein, and E. Timmermans, *Phys. Rev. A* **67**, 023606 (2003).
 - [26] F. Zhan, J. Sabbatini, M. Davis, and I. P. McCulloch, *In preparation*.
 - [27] U. Schollwöck, *Ann. Phys.* **326**, 96 (2011).
 - [28] K. Binder, *Phys. Rev. Lett.* **47**, 693 (1981).
 - [29] B. Kastening, *Phys. Rev. E* **87**, 044101 (2013).
 - [30] M. Hasenbush *J. Stat. Mech.:Theo. Exp.* P08003 (2008).
 - [31] W. Selke and L. N. Shchur, *Phys. Rev. E* **80** (2009).
 - [32] T. J. Osborne and M. A. Nielsen, *Phys. Rev. A* **66** 032110 (2002).
 - [33] G. Vidal, J. I. Latorre, E. Rico, and A. Kitaev, *Phys. Rev. Lett.* **90**, 227902 (2003).
 - [34] P. Calabrese and J. Cardy, *J. Stat. Phys.*, P06002 (2004).
 - [35] S. Östlund and S. Rommer, *Phys. Rev. Lett.* **75** 3537 (1995).
 - [36] L. Barbiero, M. Abad, and A. Recati, arXiv:1403.4185 (2014).